Septin multimer autoantibodies in severe motor neuropathy mimicking lower motor neuron disease

Friederike A. Arlt,[1,2,3,†] Ramona Miske,[4,†] Luise Appeltshauser,[2,3,5,†] Viktoria Zinnow,[2,3] Kathrin Borowski,[6] Werner Stenzel,[7] Helena Radbruch,[7] Andreas Meisel,[2,8,9] Klemens Ruprecht,[10] Matthias Endres,[2,3,8,11,12] Igor Blau,[13] Marieluise Kirchner,[14] Philipp Mertins,[14,15] Elisa Sanchez-Sendin,[2,3] Stephanie Wernick,[2,3] Hannah Pressler,[2,3] Frauke Stascheit,[2] Janis Linke,[5,16] Sophie Hümmert,[17] Hauke B. Werner,[17,18] Esravila A. Wibisono,[19] Kathrin Doppler,[5] Lars Komorowski,[4] Elias T. Spiliotis,[20] Divyanshu Dubey,[1,21] Anastasia Zeckeridou,[1,21] Sean J. Pittock,[1,21] John R. Mills,[1] Andrew McKeon,[1,21] Madeleine Scharf[4] and Harald Prüss[2,3]

[†]**These authors contributed equally to this work.**

Abstract

Severe neuropathies with predominant involvement of motor fibers can resemble lower motor neuron disease (LMND) phenotypes. Given the fatal prognosis of LMND, identifying underlying autoimmune syndromes is crucial to provide treatment options to patients.

We investigated a novel autoantibody binding pattern observed on murine teased sciatic nerve fibers. Target antigens were identified using immunoprecipitation combined with mass spectrometry. Target specificity of these autoantibodies was validated in cell-based assays, neutralization assays, and knock-out models. A retrospective study cohort consisting of different neuropathies (chronic inflammatory demyelinating polyradiculopathy n=86, Guillain-Barré syndrome n=37, multifocal motor neuropathy n=18, diabetic neuropathy n=30, other inflammatory neuropathies n=10), amyotrophic lateral sclerosis (n=50), multiple sclerosis (n=50), and healthy controls (n=50) was negative for septin multimer autoantibodies. Histopathological analysis of skin and sural nerve including electron microscopy was performed in one seropositive patient, and autoantibody binding was characterized in vitro. Extensive immunotherapy was initiated in one patient, with clinical and serological follow-up over four years.

Among 3,543 total samples tested, three patients (two male, one female) - diagnosed with the LMND variant of amyotrophic lateral sclerosis (ages 65, 72, and 79, respectively) -

showed a novel and distinct autoantibody binding pattern of indirect immunofluorescence staining on peripheral nerves, targeting Schmidt-Lanterman incisures (SLIs), paranodes, and the abaxonal myelin. Target identification and validation revealed septin multimers as autoantibody epitopes. Despite the primarily intracellular location of septins, autoantibody binding was evident in living myelinated dorsal root ganglia, primarily at SLIs ("incisuropathy"). Septin multimer autoantibodies further initiated complement deposition on fixed and permeabilized cell-based assays. Sural nerve and skin biopsies showed inflammation, myelin and axonal pathology. Extensive immunotherapy in one patient was followed by disease stabilization over three years. The other two patients died of rapid disease progression: One of them received no immunotherapy while the other had ineffective treatments with single administrations of IVIG and rituximab.

Our data suggest that septin multimer autoimmunity occurs in severe motor predominant neuropathies which can clinically resemble a neurodegenerative LMND. Screening for septin multimer autoantibodies should be considered in patients presenting with this phenotype. Follow-up studies need to determine the direct pathogenicity of septin multimer autoantibodies, their potential as a biomarker of an autoimmune syndrome, and responses to immunotherapy in larger cohorts.

Author affiliations:

1 Department of Laboratory Medicine and Pathology, Mayo Clinic, Rochester, MN 55901, USA

2 Department of Neurology and Experimental Neurology, Charité-Universitätsmedizin Berlin, corporate member of Freie Universität and Humboldt-Universität zu Berlin, 10117 Berlin, Germany

3 German Center for Neurodegenerative Diseases (DZNE) Berlin, 10117 Berlin, Germany

4 Institute for Experimental Immunology, affiliated with EUROIMMUN Medizinische Labordiagnostika AG, Seekamp 31, 23560 Luebeck, Germany

5 Department of Neurology, University Hospital Würzburg, 97080 Würzburg, Germany

6 Clinical Immunological Laboratory Prof.h.c. (RCH) Dr.med. Winfried Stöcker, 23627 Lübeck, Germany

7 Department of Neuropathology, Charité-Universitätsmedizin Berlin, corporate member of Freie Universität and Humboldt-Universität zu Berlin, 10117 Berlin, Germany

8 Center for Stroke Research Berlin, Neuroscience Clinical Research Center, Charité-

Universitätsmedizin Berlin, corporate member of Freie Universität and Humboldt-Universität zu Berlin, 10117 Berlin, Germany

9 Neuroscience Clinical Research Center, Charité-Universitätsmedizin Berlin, corporate member of Freie Universität and Humboldt-Universität zu Berlin, 10117 Berlin, Germany

10 Division of Neuroimmunology, Department of Neurology, University of Heidelberg, 69120 Heidelberg, Germany

11 German Centre for Cardiovascular Research (DZHK), partner site Berlin, 10785 Berlin, Germany

12 German Center for Mental Health (DZPG), partner site Berlin, 10117 Berlin, Germany

13 Department of Oncology and Hamatology, Charité-Universitätsmedizin Berlin, corporate member of Freie Universität and Humboldt-Universität zu Berlin, 10117 Berlin, Germany

14 Core Unit Proteomics, Berlin Institute of Health at Charité – Universitätsmedizin Berlin and Max Delbrück Center for Molecular Medicine, 10178 Berlin, Germany

15 Proteomics Platform, Max Delbrück Center for Molecular Medicine, 13125 Berlin, Germany

16 Rudolf Virchow Center, Center for Integrative and Translational Bioimaging, Julius-Maximilians-Universität Würzburg (JMU), 97080 Würzburg, Germany

17 Department of Neurogenetics, Max Planck Institute for Multidisciplinary Sciences, 37077 Göttingen, Germany

18 Faculty for Biology and Psychology, University of Göttingen, 37073 Göttingen, Germany

19 Internal Medicine, Saint Mary's Hospital, Waterbury, CT 06706, USA

20 Department of Cell Biology, University of Virginia School of Medicine, Charlottesville, VA 22903, USA

21 Department of Neurology, Center MS and Autoimmune Neurology, Mayo Clinic, Rochester, MN 55901, USA

Correspondence to: Friederike A. Arlt

Department of Laboratory Medicine and Pathology, Mayo Clinic, 200 First Street SW, Rochester, MN 55901, USA

E-mail: arlt.friederike@mayo.edu

Corresondence may also be addressed to: Harald Prüss

Charité-Universitätsmedizin Berlin, Charitéplatz 1, 10117 Berlin, Germany

E-mail: harald.pruess@charite.de

Running title: Myelin septin multimer IgGs in LMND

Keywords: motor neuron autoimmunity; autoantibody discovery; teased fiber assay; peripheral nerve inflammation

Introduction

The neurodegenerative lower motor neuron disease (LMND) variant of amyotrophic lateral sclerosis (ALS) is characterized by predominant degeneration of anterior horn cells, leading to progressive denervation, muscle weakness, atrophy, and fasciculations, ultimately resulting in respiratory failure. While LMND is driven primarily by neurodegenerative mechanisms rather than immune-mediated injury, its clinical presentation can be mimicked by severe autoimmune neuropathies and neuronopathies with predominant motor fiber involvement, such as motor-predominant chronic inflammatory demyelinating polyradiculopathy (CIDP) and bulbar anti-IgLON5 disease.[1,2] In other motor-predominant autoimmune neuropathies such as multifocal motor neuropathy (MMN) and Guillain-Barré syndrome (GBS), autoantibodies against gangliosides have been established as potent disease biomarkers facilitating timely diagnosis and care.[3] Given the fatal prognosis of LMND, identifying patients with underlying autoimmune disease mimics is crucial to provide treatment options.

Neuronally expressed SEPTIN3,-5, and -7 have been described as targets of autoantibodies in patients with various CNS autoimmune syndromes presenting with cerebellar ataxia, encephalopathy and myelopathy.[4–7] Septins are ubiquitously expressed, small guanosine triphosphate (GTP)-binding cytoskeletal proteins. Thirteen different human septin isoforms are divided into four groups based on their sequence homologies.[8] Septin monomers form hetero-hexamers or -octamers which assemble into higher-order complex cytoskeletal structures.[8] Their functions are cell- and tissue-specific varying from cell division,

polarization and migration to membrane trafficking, subcellular compartmentalization, receptor signaling, and cytokinesis.[9,10] In rodent neuronal cultures, septins function as scaffolds and diffusion barriers coordinating cytoskeletal dynamic proteins, and regulating membrane protein localization, pre-synaptic fusion and post-synaptic plasticty.[11]

In the myelin of the CNS, SEPTIN2,-4,-7, and -8 assemble into filaments.[12] These complexes are necessary for myelin integrity as oligodendroglial deficiency of myelin septin filaments causes pathological myelin outfoldings and reduced nerve conduction velocity in mice.[12,13] In the peripheral nervous system (PNS) however, the relevance of septins for myelin formation and maintenance remains largely unknown.[14] Further, PNS-reactive autoantibodies targeting septins have not been described to date. Here, we report the identification of a novel type of septin autoantibody, targeting myelin septin multimers in patients with severe inflammatory neuropathies presenting as neurodegenerative LMND.

Materials and methods

Study participants, anti-neuronal antibody screening, and retrospective cohort screening

Patients included in the study were referred to *Charité Berlin*, or to Mayo Clinic, Rochester for anti-neuronal antibody testing. Sera were tested on indirect immunofluorescence assays (IIFA) using mouse brain and nerve tissue as part of diagnostic workup. At *Charité*, the brain IIFA is performed on a research basis using an in-house assay with unfixed whole mouse brain sections and sera were diluted at 1:200. The index case was identified in collaboration with *EUROIMMUN* among 727 consecutive samples tested in 2021 (cohort 1). Additional cases were identified by applying predefined criteria consisting of 1) the characteristic brain IIFA staining pattern as used in routine clinical testing at the Neuroimmunology Laboratory of Mayo Clinic Rochester, one of the highest-throughput laboratories worldwide, and 2) the absence of septin monomer reactivity in cell-based assays (CBA). At Mayo Clinic, the IIFA is conducted on a validated clinical assay using composite brain tissue slides (#0832-M-BR, Medica Scimedx Corporation, Dover, NJ, USA) at a serum dilution of 1:240. Two additional cases were identified across two independent cohorts that were sent to *EUROIMMUN* for septin multimer antibody testing (total amount of samples tested n=2,816 (cohort 2 was previously published[15])). The two additionally identified patients were also tested on a peripheral nerve tissue IIFA research-use assay with sciatic nerve teased fibers of mice. For detailed protocols of IIFAs at *Charité* (brain and sciatic nerve), Mayo Clinic (brain and sciatic nerve), and *EUROIMMUN* (brain) as well as the

flowchart and description of case identifications refer to the Supplementary Material.

Following the identification of three cases with a shared novel autoantibody, we retrospectively screened in defined cohorts of patients with ALS fulfilling El-Escorial criteria (n=50), CIDP fulfilling 2021 CIDP criteria[16] (n=86), GBS (n=37), MMN (n=18), diabetic polyneuropathies (n=30), and patients with other neuropathies (n=10) for septin multimer autoantibodies using brain and nerve tissue IIFA, as well as CBAs expressing septin multimers. Further, healthy controls (n=50) were tested on the research-based assays. Septin multimer autoantibody CBA specificity was further investigated using a disease control cohort of multiple sclerosis patients (n=50).

Animals

Tissue collection from male C57BL/6 and *Septin7*$^{flox/flox}$*; Cnp*^{Cre} mice followed German animal welfare law (TierSchG §4) and was approved by the *Landesamt für Gesundheit und Soziales (LaGeSo)* in Berlin (approval number T-CH 0009/22), and the *Niedersächsisches Landesamt für Verbraucherschutz und Lebensmittelsicherheit (LAVES)*. *Septin7*$^{flox/flox}$*; Dhh*^{Cre} mice (see below) were bred and kept in the mouse facility of the Max Planck Institute for Multidisciplinary Sciences, Göttingen, Germany (MPI-NAT) in accordance with the German animal protection law (TierSchG) and approved by the *Niedersächsisches Landesamt für Verbraucherschutz und Lebensmittelsicherheit (LAVES)*. For the procedure of sacrificing vertebrates for preparation of tissue, all regulations given in the German animal welfare law (TierSchG §4) are followed. Since sacrificing of rodents including E16 embryos for tissue collection or cell culture is not an experiment on animals according to §7 Abs. 2 Satz 3 TierSchG, no specific ethical review and approval is required for the present work. All procedures were supervised by the animal welfare officers. The animal facilities are registered according to §11 Abs. 1 TierSchG.

Deletion of *Septin7* in Schwann cells of mice

To delete the *Septin7* gene in Schwann cells, *Septin7*$^{flox/flox}$ mice[17] were interbred with mice expressing *Cre* under control of the *Cnp* promoter[18] yielding *Septin7*$^{flox/flox}$*;Cnp*^{Cre} mice, also termed *Septin7*-cKO, and respective *Septin7*$^{flox/flox}$ controls without *Cre*. Genotyping was carried out by genomic PCR.

Genotyping of *Septin7*-cKO, and respective *Septin7*$^{flox/flox}$ mice

Septin7 genotypes were identified using primers 5'-GGTATAGGGG ACTTTGGGG, 5'-CTTTGCACAT ATGACTAAGC, and 5'-GCTTCTTTTA TGTAATCCAGG, yielding a 151 bp product for the wildtype allele, a 197 bp product for the unrecombined *Septin7*^{flox} allele, or a 256 bp product for the recombined *Septin7*^{flox} allele. PCR genotyping of the *Cnp* allele was performed with primers 5´-GCCTTCAAAC TGTCCATCTC, 5´-CCCAGCCCTT TTATTACCAC, 5´-CCTGGAAAAT GCTTCTGTCCG, and 5´-CAGGGTGTTA TAAGCAATCCC as previously described.[12] Three mice per genotype (cKO and flox/flox littermates) were used for IIFA experiments on sciatic nerve teased fibers as described below.

Mouse sciatic nerve teased fibers

Preparations of mouse sciatic nerve teased fibers were conducted as previously described.[19] In brief, wildtype (WT) mouse sciatic nerves were freshly prepared, and immediately fixed in 4% PFA for 20min on ice. Epineuriums were removed, and single fibers were teased on glass slides. Slides were air-dried, frozen at -20°C, and used within 14 days for IIFAs.

Indirect immunofluorescence assay

IIFAs on brain tissue performed at *Charité*, Mayo Clinic, and *EUROIMMUN* including the neutralization assays, as well as the confocal colocalization studies are described in detail in the Supplementary Material. IIFAs on sciatic nerve teased fibers were performed as previously described.[19] In brief, slides were permeabilized with MeOH for 3min at -20°C or 0.1% Triton-X for 3min at room temperature (RT), and washed with PBS. After blocking with blocking solution (10 % normal goat serum, 2.5 % bovine serum albumin) for 1h at RT, sera (dilution 1:500) or commercial primary antibodies against SEPTINs (SEPTIN2 - #ab179436, abcam, Cambridge, UK, 1:50; SEPTIN7 - #18991, IBL-Tecan, Switzerland, 1:20) were added over night at 4°C. After washing, secondary antibodies against human IgG labeled with Alexa-488 (#109–545-003, Dianova, Hamburg, Germany, 1:1,000) or against rabbit IgG labeled with Alexa-594 (#111-585-003, JacksonImmunoResearch, Westgrove, Pennsylvania, U.S., 1:500) were added for 2h at RT. Slides were mounted in mounting media and kept at 4°C.

Recombinant expression of SEPTIN proteins in HEK293 cells and fixed cell-based assays

The expression of SEPTIN monomers (3,5,6,7,11) and successful multimer expression was described previously[4] and accordingly performed in this work. Additionally, SEPTIN2 monomers were expressed using a commercially available full-length plasmid

(#RC224864, Origene, Rockville, MD, USA). HEK293 cells were transfected at a confluency of 60-70% in 50% of regular growth media volume using Polyethylenimine (PEI, #26008, Kyfora Bio, Horsham PA, USA) with a 1:5 DNA:PEI ratio. The day after transfection, growth media was added to reach 100% of the final volume. For multimer expression, equal amounts of DNA of each monomer were used to accomplish complex expression (e.g. for SEPTIN3,5,6,7,11: 0.2µg of DNA for each monomer leading to a total of 1µg DNA in the transfection reagent). 48h after transfection, cells were fixed with acetone and subjected to immunofluorescence staining using serum and secondary anti-human antibodies. Sera were diluted 1:100 for screening experiments and diluted further to reach endpoint-titers. Sera were diluted in PBS-Tween and added to the transfected and acetone-fixed cells for 30min at RT. After 5min of washing with PBS-Tween, cells were incubated with anti-human Pan-IgG secondary antibodies labelled with FITC (*EUROIMMUN Medizinische Labordiagnostika AG*, Luebeck, Germany, undiluted). For IgG subclassification, we used subclass-specific secondary antibodies (Sigma-Aldrich F0767, F4516, F4641, F9890, 1:25).

Live HEK293 cell-based assays

Recombinant expression of SEPTIN3,5,6,7,11 multimers was performed as described above. 48h after transfections, transfected cells and control cells were incubated with PBS-diluted serum (1:20) for 30min on ice or with a commercial anti-SEPTIN antibody mix consisting of anti-SEPTIN3,6,7,11 (SEPTIN3 #30146-1AP, Proteintech, Rosemont, IL, USA; SEPTIN6 #12805-AP, Proteintech SEPTIN7 #18991, IBL-Tecan, Switzerland, 1:20, SEPTIN11 #14672-1-AP, Proteintech, final dilution 1:20 in PBS). After washing with PBS, cells were stained with secondary anti-human or anti-rabbit Pan-IgG antibodies labeled with FITC (#2040-02 Southern biotech, AL, USA, 1:200) or TRITC (#4050-03, Southern biotech, 1:200) for 30min on ice. Cells were washed with PBS and fixed with MeOH for 3min at -20°C. Subsequently, cells that were stained with sera were blocked with blocking solution for 1h at RT. The commercial anti-SEPTIN antibody mix (anti-SEPTIN3,6,7,11) was added in a dilution of 1:100 in blocking solution at 4°C over night. After washing with PBS, secondary anti-rabbit antibodies labeled with TRITC (Southern biotech) were added in a dilution of 1:200 for 1h at RT. Cells were resuspended in PBS and imaged within plates with optical dense plastique bottoms on a confocal microscope.

Complement deposition assay on fixed HEK293 cell-based assays

For the complement deposition assay, acetone-fixed septin multimer (3,5,6,7,11) overexpressing HEK293 cells were used as cell-surface expression of septin multimers could not be achieved (see Supplementary Fig. 4). Patient serum incubation (30µl, dilution 1:10) was followed by complement (*EUROIMMUN*, ZF 9000-0002, 25µl) incubation for 30min at RT, and a PBS-Tween wash. To visualize binding of human IgGs to septin

multimers and deposition of complement, a directly labeled anti-human-C3c-FITC antibody *(EUROIMMUN*, AF 612-0115, undiluted) and anti-human-IgG-Cy3 antibody (JacksonImmunoResearch, 1:400) were incubated simultaneously for 30min at RT. Fluorescent colours of patient IgG and C3c signals were retrospectively adjusted to keep colouring consistent throughout the manuscript.

Immunoprecipitation coupled to mass spectrometry (IP-MS)

IP-MS was performed as previously described.[20] In brief, sciatic nerves of WT mice were solubilized in lysis buffer. Sera were bound to Dynabeads™ Protein G (#10004D, Invitrogen, Vilnius, Lithuania), and incubated with the cleared lysates. After washing, we performed on-bead digestion with LysC and trypsin, followed by ms-based proteomic analyses employing liquid chromatography tandem mass spectrometry (LC-MS/MS). The raw data were processed using the MaxQuant software package with human and mouse UniProt databases (HUMAN.2020-06; MOUSE.2019-07). Label-free quantitation intensities were utilized for statistical analyses. For target identification, group comparisons against the negative control were employed using Student's T-test, with a significance threshold set at a false discovery rate (FDR) of 5%.

Binding assays on living myelinated dorsal root ganglion cultures

Murine myelinating organotypic dorsal root ganglion explant co-cultures were cultured and assessed as previously described.[21] Cells were cultured for 20 days to achieve compact myelination including Schmidt-Lanterman Incisures (SLIs) and nodes of Ranvier. They were either fixed and co-stained with serum and commercial antibodies, or living cells were incubated with filtrated serum (1:100) in myelination medium for two or five days, before fixation and co-staining with anti-human IgG. Immunofluorescence was performed as described previously[21] using antibodies against SEPTIN7 (1:20), SEPTIN2 (1:100), Neurofascin (#AF3235, R&D Systems, Minneapolis, U.S., 1:5000), and myelin associated glycoprotein (# MAB1567, Merck, Darmstadt, Germany, 1:1500), along with appropriate secondary antibodies. All experiments were performed twice.

Immunofluorescence analysis of skin

Dermal punch biopsies from the lateral index finger and the leg were stained with anti-MBP (#GTX133108, GeneTex, 1:200) and anti-Neurofascin (R&D Systems, 1:400), and anti-Caspr1 (#ab34151, Abcam) as previously described.[22]

Morphologic analysis of sural nerve and skin biopsies

Diagnostic conventional histology and enzyme histochemistry reactions (H&E, Gömöri trichrome, acid phosphatase, Elastica van Gieson, Kongo red, CD3, CD8, CD31, CD45,

CD68, C5b-9, CD20, CD138, neurofilament) were performed on 8µm thick cryostat sections according to international recommendation and as previously described.[23,24] Teased fiber preparations from the sural nerve were conducted according to established protocols.[25]

Electron microscopy of sural nerve biopsy

Nerve tissues were fixed with 2.5% glutaraldehyde in 0.1M sodium cacodylate buffer, postfixed with 1% osmium tetroxide in 0.05M sodium cacodylate, dehydrated and embedded in Renlam resin. Uranyl acetate and phosphotungstic acid were used for contrasting. 70nm ultrathin sections were cut using an ultramicrotome, stretched with xylene vapor, collected onto pioloform-coated slot grids and stained with lead citrate. Transmission electron microscopy was performed using a Zeiss 906 microscope with a 2k CCD camera (TRS).

Ethics and study approval

The study was conducted in accordance with the declaration of Helsinki. All participants gave written informed consent for study participation and serum biomarker analyses. The study was approved by the ethics board of *Charité* (#EA1/258/18) and Mayo Clinic Rochester (IRB #23-007528 and #21-1297).

Software and Data visualization

Microscope images including maximum projections of z-stacks were processed using the FIJI software[26,27], Imaris Version 9.9.1 (Bitplane, Belfast, U.K.). Data visualization was performed in Prism Version 9.4.1 (GraphPad Software, San Diego, CA), Inkscape Version 1.2.1 (Inkscape Project. 2020, https://inkscape.org), Illustrator (Adobe Inc., San José, CA, U.S.), and using Biorender.com.

Results

Suspected LMND patients exhibit autoantibodies against SLIs, paranodes, and abaxonal myelin

The here-reported patients showed a positive autoantibody result on brain and nerve tissue, revealing a previously undescribed binding pattern on teased nerve fibers. The index patient was referred to *Charité Berlin* (among a total of 727 consecutive samples tested in 2021) while the other two patients were found via retrospective screening (total amount of

samples tested n=2,816). For additional detailed information on the identification of all three cases refer to the flowchart (Supplementary Fig.1) and the description in the Supplementary material. All three patients (two males, one female), aged 65, 72 and 79 years at symptom onset, presented with fine motor skill impairment, progressive and severe, asymmetric, distally predominant muscle weakness, and atrophy with fasciculations and limb cramps, predominantly affecting the lower limb in patient 1 and 3, and the upper limb in patient 2. Disease progression was rapid in patient 3, moderate in patient 2, and relatively slow in patient 1. From symptom onset to requiring a wheelchair ambulance, patient 1 deteriorated over three years, whereas patient 3 became wheelchair-bound within just four months.

Patient 1 and 3 initially complained of sensory symptoms, which were right-dominant distal hypoesthesia for touch, temperature, and pain sensation starting in both legs in patient 1, and paresthesia (pins and needle sensation) in both legs and feet in patient 3. None of the patients had neuropathic pain. Bulbar involvement with dysphagia and intermittent aspirations developed in patient 1 (late in the disease course) and within months in patient 3, while information on bulbar function was not available for patient 2.

Electrophysiological studies in all patients showed distal axonal and motor-predominant neuropathy with accompanying demyelinating features, (reduced nerve conduction velocity in one nerve in patient 1 and prolonged distal motor latencies in two nerves in patient 3). Sensory nerve conduction studies showed abnormalities in 2-3 nerves in patients 1 and 3. Thus, those two patients fulfilled electrodiagnostic criteria [16] for (possible) multifocal CIDP, but clinical criteria for multifocal CIDP were not met due to the lack of additional suggestive criteria (patient 1), normal tendon reflexes (patient 3) and a clinically more probable differential diagnosis. No conduction blocks suggestive of MMN were present. Axonal damage increased over time in patient 1 where longitudinal data on electrophysiology was available (Supplementary Tables 1 and 3). Electromyography showed active denervation, and pathological spontaneous activity in the extremities and paravertebral muscles of patient 1 and 2 (Supplementary Table 2). Spinal cord imaging remained without inflammatory correlates of symptoms in all three patients. CSF status revealed a minimal protein elevation in patient 2 and patient 3 while other CSF status parameters were normal. For additional detailed clinical data, refer to Table 1. In all three patients, an axonal-demyelinating neuropathy was initially suspected, and autoimmune etiology was considered by the treating physicians who initiated testing for autoantibodies. Patient 2 and 3 both showed a low-titer positive VGCC-P/Q test result (0.05nmol/L, reference <0.02nmol/L) while other autoantibody panel testing remained negative (Supplementary Table 4). Due to asymmetric and partial upper limb presentation, signs of paravertebral and bulbar denervation, motor predominance with evolving and severe

muscle atrophy, and moderate to rapid disease progression despite initial trials of IVIG therapies (in patients 1 and 3), all three patients were ultimately diagnosed with the LMND variant of ALS.

The novel binding pattern of autoantibodies on teased nerve fibers involved the abaxonal myelin, the paranodes and SLIs (Fig. 1A), which was not detected in healthy controls (n=50).

Autoantibodies target septin multimers in PNS myelin

To identify the autoantibody targets, we used the index patient serum (patient 1) and applied two parallel strategies: CBAs expressing different neuronal antigens, and an untargeted approach using IP-MS with sciatic nerve lysate. IP-MS revealed binding to several septin proteins (Fig. 1B). Among them, SEPTIN2 and SEPTIN7 had the highest protein abundance (Fig. 1C). Interestingly, different to septin autoantibodies described previously[4–6], the sera of all patients showed no or only weak reactivities with several septin monomers (SEPTIN2,-3,-5,-6,-7, or -11, SupplementaryFig. 2A). Overexpression of septins in a multimer (constituted of SEPTIN3,-5,-6,-7,-11) however showed strong binding of the patients' autoantibodies (Fig. 1D, serum titer of 1:320,000 in patient 1 and 1:100,000 in #2 and #3). Septin multimer reactivities in CBA could not be abolished by depletion of one of the septins from the multimer (SupplementaryFig. 2B). Testing of the patients' sera on protein microarray displaying full-length human proteins showed no binding to single septins, further suggesting that no linear epitope to septin proteins is detected (Supplementary Fig. 2C). Sera also reacted with rat brain sections in the hippocampus and the cerebellum showing a characteristic septin staining pattern[4–6] (Fig. 1E-F) and additionally showed white matter reactivity (Fig. 1F). Tissue reactivity was abolished by preincubation of patients' sera with HEK cell extracts expressing SEPTIN3,-5,-6,-7,-11 multimers (Fig.1G). In contrast, pre-adsorption using SEPTIN3 or -7 alone did not abolish tissue binding (Supplementary Fig. 3A). Further, heat-denatured HEK cell extracts expressing SEPTIN3,-5,-6,-7,-11 multimers did not neutralize tissue binding, and neither did a mixture of HEK cell extracts expressing SEPTIN3,-5,-6,-7,-11 monomers (Supplementary Fig. 3B and C). A bacterially expressed and purified hetero-octamer consisting of SEPTIN2,-6,-7, and -9 was similarly effective in abolishing tissue binding as the HEK cell extracts expressing the SEPTIN3,-5,-6,-7,-11 multimers (Supplementary Fig. 3D). Taken together, these findings confirm that a conformational epitope only present after septin multimer formation is recognized.

Staining patterns of septin autoantibodies have so far not been described on peripheral

nerves. Here, serum binding colocalized with anti-SEPTIN2 and anti-SEPTIN7 commercial antibodies at the paranodal myelin of large caliber fibers (Fig. 2A), the paranode of small caliber fibers (Fig. 2B), and the SLIs of myelinated fibers (Fig. 2C). To investigate binding properties to peripheral nerve myelin deficient of septin proteins, we bred mice in which a floxed allele of the *Septin7* gene[17] is recombined by Cre recombinase in Schwann cells under control of the *Cnp*-promoter.[28] Indeed, *Septin7*-cKO (conditional knock-out) mice lack both *Septin7* (Fig. 2D) and *Septin2* (Supplementary Fig. 4A) immunolabelling from Schwann cells, and thus presumably the entire myelin septin multimer.[14] Here, patient serum reacted weakly with the axon while binding to paranodes, abaxonal myelin, and SLIs was lost in *Septin7*-cKO mice (Fig. 2E) as opposed to their flox/flox littermates (Supplementary Fig. 4B). Weak immunolabeling of SEPTIN7 in cKO axons was shown using the commercial SEPTIN7 antibody (Fig. 2F). In line with CNS pre-adsorption, IgG signals were lost on sciatic nerves upon pre-adsorption of sera with SEPTIN3,-5,-6,-7,-11 multimers (Fig. 2G, serum inserts). On a control human sural nerve biopsy, anti-SEPTIN7 staining confirmed the distribution of septin proteins in human nerves (Supplementary Fig. 4C).

Septin multimer autoantibodies penetrate the node of Ranvier and SLIs in cultured DRG neurons

Nodo-paranodal structures and SLIs are hard to reach by autoantibodies.[29,30] To assess binding to these structures in living and unfixed neurons, we performed pre-incubation assays on live murine myelinating dorsal root ganglion cell (DRG) cultures (Fig. 3 and Supplementary Videos 1 and 2).

On non-fixed, non-permeabilized myelinated cultures, no binding was observed after a short incubation of 1h. After two incubation days, slight IgG deposition at the SLIs and paranodes was present with serum 1, but not with control serum, with increasing intensity after five days (Fig. 3A-C). Binding partially colocalized with SEPTIN7 and SEPTIN2, especially at the paranodal region (Fig. 3A-B). The staining with commercial anti-SEPTIN7 and SEPTIN2 was slightly weaker after preincubation with patient serum compared to the control serum, indicating either epitope masking or target antigen internalization (Fig. 3A-B). Strong binding of patient serum to paranodes and SLIs could also be detected when incubating after fixation and permeabilization of the cells (Fig. 3C). Unspecific binding to fibroblasts and cells in the culture was likewise observed in healthy controls (Supplementary Videos 1 and 2, available at Zenodo, doi:10.5281/zenodo.20059953 and doi:10.5281/zenodo.20101101). Alterations to nodo-paranodal structures, myelin and SLI could not be detected within the incubation of five days (see co-staining with antibodies

against myelin-associated glycoprotein and Neurofascin, Fig. 3C and Supplementary Video 2). In septin multimer overexpressing HEK cells, however, no live-cell binding of serum was evident (Supplementary Fig. 6).

Hence, despite their intracellular location, septin multimer autoantibodies reach their target in vitro and predominantly bind to SLIs, where native cellular structure and epitopes are presumably preserved.

Complement deposition and immune cell infiltration in sural nerve biopsy

IgG-subclass determination revealed predominance of the complement fixing IgG3- and IgG1-subclasses (patient 1: IgG3>IgG1, patient 2: IgG3=IgG2>IgG1, patient 3: IgG1; data not shown). Further, we observed antigen-dependent complement deposition of cleaved complement component 3 (C3c) on fixed septin multimer overexpressing HEK cells upon incubation of serum 1 in contrast to the non-binding healthy control (Fig. 4A). In line, membrane attack complex (MAC) deposition (illustrated via C5b-9) was visible in the sural nerve biopsy of patient 1 located at endoneurial capillaries (Fig. 4B). Moreover, histopathological analysis of the sural nerve biopsy showed edematous changes and inflammatory infiltrates, predominantly in the perineurium (Fig. 4C).

Histopathological and ultrastructural in vivo evidence of axonal degeneration, and de- and remyelination

Despite the absence of immediate structural effects by septin multimer autoantibodies on live DRG cultures, signs of severe de- and remyelination were evident in the sural nerve biopsy of patient 1 with hypomyelinated axons, regenerating fibers, next to acute axonal degeneration [Fig. 5A(i and ii)]. Teased fiber preparation revealed acute axonal damage and some segmental demyelination, while nodal regions did not show distinct pathological changes, specifically no enlargement of the nodal gap [Fig. 5B(i and ii)]. EM analysis showed loss of primary unmyelinated axons with formation of collagen bundles surrounded by Schwann cell processes (Fig. 5C). In the skin, fibers showed partially decreased myelin staining (Fig. 5D), as well as elongated nodes of Ranvier in some fibers (Fig. 5E). However, normal fibers with regular myelin and intact nodal architecture were similarly present (Fig. 5F). Intraepidermal nerve fiber density was normal (data not shown). Taken together, morphological analysis of the sural nerve and the skin revealed myelin pathology next to axonal degeneration while the nodal regions were only partially abnormal.

Clinical specificity of septin multimer antibodies

Accounting for the relevance of tissue reactivity, retrospective testing for septin multimer autoantibodies in different cohorts with motor-predominant neuropathies was performed using fixed CBAs, as well as brain and nerve tissue IIFAs. No additional case with septin multimer autoantibodies was detected in CIDP (n=86), MMN (n=18), GBS (n=37), or ALS (n=50). Additional neuropathy cohorts with diabetic neuropathies (n=30), and other inflammatory neuropathies (n=10) also remained without septin multimer autoantibody cases (Supplementary Fig. 5 and Supplementary Table 4). These findings indicate that septin multimer autoantibodies as detected by tissue IIFA and CBA are rare, but specific.

Immunotherapy likely stabilized disease progression

Based on these findings, we initiated extensive immunotherapy in patient 1, including plasma exchange (PE), B-cell and plasma cell depletion (rituximab, daratumumab), autologous stem cell transplantation, and complement inhibition (ravulizumab). PE was followed by immediate improvement in hand muscle strength (Fig. 6A) and a subjective reduction in sensory deficits. With intensified treatment, his overall condition stabilized at a low functional level (mRS = 4), corresponding with a decline in CBA titers (Fig. 6B–C). However, slow progression of muscle weakness over subsequent years could not be fully halted (data not shown), parallel to continuous autoantibody presence in serum (Fig. 6C). Patient 2 died two years after symptom onset, before the discovery of the septin multimer autoantibodies (Fig. 6B). Patient 3 received a trial of IVIG, and a single dose of rituximab based on a low-positive VGCC-P/Q antibody result (0.05 nmol/L; reference <0.02 nmol/L), but without any apparent clinical benefit (data not shown). The patient ultimately opted for hospice care before the septin multimer autoantibody was identified and died 14 months after disease onset.

Discussion

We identified autoantibodies targeting septin multimers in peripheral nerve myelin. Three patients harboring these autoantibodies were diagnosed with the LMND variant of ALS. While two patients did not receive effective intensified immunotherapy and died from rapidly progressing disease, one patient was extensively treated followed by stabilization of disease for several years. Experimental data showed that these autoantibodies reached

SLIs and paranodes in vitro and initiated complement deposition, compatible with a potential pathogenic role. In vivo data from sural nerve and skin biopsies revealed inflammation as well as myelin and axonal pathology.

The concept of autoreactive antibodies targeting the node of Ranvier is well-established[31,32] and autoantibody-targeted therapy with PE and rituximab in autoimmune nodopathies has shown beneficial effects.[32] The autoantibodies identified in this work, however, differ in several aspects from the autoantibodies targeting, for example, pan-Neurofascin or Contactin-1. While these antibodies bind the node[21,33], are often of IgG4-subclass[34], target extracellularly located proteins, and lead to immediate and direct pathological changes in (para)nodal ultrastructure[21,29], autoantibodies targeting intracellularly located septin multimers bound primarily to SLIs and paranodes, were predominantly of IgG3- and IgG1-subclass, and showed no immediate effect in cultured myelinating DRGs. In line, the clinical presentation of all three patients suggests a chronic progressive process without definitive improvement upon treatment but rather disease stabilization, whereas autoimmune nodopathies usually present as (sub)acute demyelinating inflammatory neuropathies with good immediate response to appropriate immunotherapy.[31,35]

Septin multimers represent intracellular antigens; however, both our work and a previous study[6] demonstrate their accessibility in live-cell systems. The work by Hinson et al. showed live-cell binding to primary hippocampal neuronal cultures and demonstrated functional effects for septin autoantibodies targeting neuronally expressed septin monomers. We also observed neuronal binding in live-cell neuronal cultures (Supplementary Fig. 4) supporting the accessibility of septin multimers in neuronal and myelinating cells. In contrast, no live-cell binding was observed in an artificial HEK293 cell overexpression system, suggesting that extracellular accessible epitopes might only be presented in the native cellular context.

Previous studies demonstrate that myositis-specific autoantibodies, including anti-SRP and anti-HMGCR, can be pathogenic by not only inducing muscle damage in vivo through passive transfer but also by being internalized into muscle fibers where they disrupt intracellular targets, establishing a causal role for autoantibodies against intracellular antigens in myositis pathogenesis.[36,37] These findings support the broader concept that antibodies against non-cell-surface proteins can exert pathogenic effects. However, direct proof of autoantibody-mediated pathophysiology of the here-described autoantibodies is still lacking. Even in the absence of direct pathogenicity, autoantibodies against intracellular antigens have been established as robust biomarkers in several autoimmune diseases. Accordingly, the absence of septin multimer autoantibodies in multiple disease cohorts supports their potential utility as a disease-specific biomarker.

One of the predominant binding site of the autoantibodies described here within the PNS is the SLI. Further, the available nerve biopsy revealed distinct immune-mediated abnormalities including features of de- and remyelination but also extensive axonal damage. These findings raise the possibility that a long-term demyelinating and subsequent early axonal degeneration process could be initiated at and spread from the SLIs. Septin multimer autoantibodies may thus define a novel subgroup of autoantibody-associated neuropathies, which could be termed *"incisuropathies"*, characterized by impaired metabolic exchange and/or disruption of myelin structural integrity potentially leading to early axonal irreversible damage.

The direct effect of septin deficiency or overexpression in PNS myelin is largely unexplored. Septin abundances are altered in genetic demyelinating neuropathy mouse models[38,39] and *Septin9* mutations cause hereditary neuralgic amyotrophy[40,41], often associated with prominent axonal damage in electrophysiology[42]. However, mice lacking *Septin2* or *Septin9* specifically in Schwann cells did not show an evident neuropathic phenotype.[14] Long-term effects (>one year) such as maintenance of myelin integrity were however not investigated in *Septin2*-cKO or *Septin9*-cKO mice[14], nor in our cultured DRGs upon autoantibody incubation. Yet a potential function of septins on PNS myelin maintenance (rather than development) appears possible when considering their function in the maintenance of CNS myelin structure.[43]

Complement plays a key role in several autoantibody-mediated neuropathies, including myasthenia gravis, where its inhibition is effective in treatment.[44,45] Septin multimer autoantibodies were mainly IgG3, a complement-activating subclass previously linked to severe autoimmune nodopathies with Pan-Neurofascin and Contactin-1 IgG3 and fulminant course.[46,47] The nerve biopsy showed inflammation including endoneurial capillary complement deposition. Although overlapping with further immunotherapies, patient 1 received complement inhibitors (ravulizumab), and intermittent clinical stabilization might have suggested a contribution to disease pathology.[46,47]

However, extensive treatment in one patient including complement inhibition, could not reverse the clinical course, consistent with early axonal damage, advanced atrophic paresis, and persistent high autoantibody titers. Earlier autoantibody testing and aggressive intervention might have prevented irreversible damage, underscoring the value of early biomarker screening.

Limitations

Septin multimer autoantibodies seem to be rare as only three cases were identified within different neuroimmunology laboratories over several years, thus limiting the generalizability

of our findings given the small number of patients reported. Neuropathic features in large motor fibers could not be assessed, and direct autoantibody pathogenicity remains unclear, as no motor nerve cell culture model or animal testing was conducted. The complement deposition assay was performed on fixed cells overexpressing septin multimers as cell surface expression could not be achieved in this system, thereby limiting the interpretation regarding potential complement activation in vivo. Further, IP-MS, HEK live-cell, DRG and complement studies were restricted to one serum sample due to limited availability of serum 2 and 3.

Conclusion

Septin multimer autoantibodies may occur in motor-predominant and severe neuropathies. Immunotherapy should be considered if signs of inflammatory demyelination are seen in electrophysiology or histology. Future studies should clarify their frequency and relevance as biomarkers and assess pathogenicity using patient-derived monoclonal antibodies or active immunization in animal models, as well as therapy responses in larger cohorts.

Data availability

Data is available from the principal investigator upon reasonable request.

Acknowledgements

We are grateful for the excellent technical assistance of Jakub Korytkowski, Cordula zum Bruch and Ramona Jung in the preparation of teased fibers and Barbara Reuter for excellent technical assistance with cell culture and immunostainings. We thank Matthias Gaestel and Alexey Kotlyarov for mice comprising the *Septin7*-flox allele. The thumbnail image for the online table of contents was created in BioRender. Arlt, F. (2026). https://BioRender.com/s1w5kjd

Funding

This work was supported by grants from the German Research Foundation (DFG; Clinical

Research Unit KFO 5023 'BecauseY' [project number 504745852], grants FOR3004, PR1274/5–1, and PR1274/9–1), by the Helmholtz Association (HIL-A03 BaoBab), and by the German Federal Ministry of Education and Research (Connect-Generate 01GM1908D) to HP. L.A. was supported by the Interdisciplinary Center of Clinical Research (IZKF) of the Faculty of Medicine, University of Würzburg (#ZZ-32). A.M. received speaker or consultancy honoraria or financial research support (paid to his institution) from Alexion, argenx, axunio, Desitin, Grifols, Hormosan, Pharma, Janssen, the healthcare business of Merck KGaA, Darmstadt, Germany, Novartis, Octapharma, Sanofi, and UCB. K.R. received research support from Novartis, Merck Serono, German Ministry of Education and Research, European Union (821283-2), Stiftung Charité, Guthy-Jackson Charitable Foundation and Arthur Arnstein Foundation; received travel grants from Guthy-Jackson Charitable Foundation and speaker's honoraria from Virion Serion and Novartis; was a participant in BIH Clinical Fellow Program funded by Stiftung Charité. M.E. received funding from DFG under Germanys Excellence Strategy – EXC-2049 – 390,688,087, Collaborative Research Center ReTune TRR 295—424778381, Clinical Research Group KFO 5023 BecauseY, project 2 EN343/16-1, BMBF, DZNE, DZHK, EU, Corona Foundation, and Fondation Leducq. H.B.W. is supported by the Deutsche Forschungsgemeinschaft (DFG grant WE 2720/2-2). A.McK. is funded by NIH (RO1NS126227). E.T.S. is funded by NIH grant 2R35GM136337-07 from the National Institute of General Medical Sciences. H.R. received funding from German Research Foundation (DFG; Clinical Research Unit KFO RA 2491/4-1).

Competing interests

R.M., M.S. and L.K. are employees of EUROIMMUN, a company that manufactures diagnostic tests and instruments. R.M., M.S. and L.K. have septin-3 and -7 patent applications pending. A.McK. reports patents issued for GFAP and MAP1B-IgGs and patents pending for Septins-5 and -7, and KLHL11-IgGs, and has consulted for Janssen and Roche pharmaceuticals, without personal compensation. A.Z. reports has patents submitted for DACH1-IgG, PDE10A-IgG, CAMKV-IgG, Tenascin-R-IgG as biomarkers of neurological autoimmunity. She has received research funding from Roche/Genetech and Center for MS and Autoimmune Neurology at Mayo Clinic. She has consulted without personal compensation for Alexion pharmaceuticals. S.J.P. reports reports grants, personal fees, and non-financial support from Alexion Pharmaceuticals; grants, personal fees, and non-financial support from Amgen; and personal fees for consulting from Genentech, Roche, UCB, and Arialys. He has two patents issued (8,889,102; application 12–678,350;

Neuromyelitis Optica Autoantibodies as a Marker for Neoplasia; and 9891219B2; application 12–573,942; Methods for Treating Neuromyelitis Optica [NMO] by Administration of Eculizumab to an individual that is Aquaporin-4 [AQP4]-IgG Autoantibody positive) for which he has received royalties. He also has patents pending for IgGs to the following proteins as biomarkers of autoimmune neurological disorders: septin-5, kelch-like protein 11, LUZP4, PDE10A, and MAP1B. D.D. reports has served on the clinical advisory board for UCB, Argenx, and Arialys Pharmaceuticals, with all compensation for consulting activities being paid directly to Mayo Clinic. He is a named inventor on a filed patent that relates to KLHL11 as a marker of autoimmunity and germ cell tumor. Additionally, he has patents pending for LUZP4-IgG, cavin-4-IgG, and SKOR2-IgG as markers of neurological autoimmunity. He has received funding from the DOD (CA210208 [germ cell tumor], PR220430 [inflammatory neuropathy], and AL240239 [ALS]), the David J. Tomassoni ALS Research Grant Program, and UCB. J.R.M. reports grant support from Werfen Diagnostics. He has patents issued related to the measurement of immunoglobulins by mass spectrometry for which he receives royalties. He also has patents pending for LUZP4-IgG, Cavin-4-IgG, and SKOR2-IgG as markers of neurological autoimmunity. F.S. received travel/accommodation/meeting expenses from Alexion Pharmaceuticals and argnx and received speaking honoria and honoria for attendance at advisory boards from Alexion Pharmaceuticals, argnx and UCB pharma. She receives financial research support (paid to her institution) from Alexion Pharmaceuticals, Cytel and Argenx. She serves as a member of the medical advisory of the German Myasthenia Gravis Society e.V.

Supplementary material

Supplementary material is available at *Brain* online.

References

1. Kwan J, Vullaganti M. Amyotrophic lateral sclerosis mimics. *Muscle Nerve*. 2022;66(3):240-252. doi:10.1002/mus.27567

2. Werner J, Jelcic I, Schwarz EI, et al. Anti-IgLON5 Disease: A New Bulbar-Onset Motor Neuron Mimic Syndrome. *Neurol Neuroimmunol Neuroinflamm*. 2021;8(2):e962. doi:10.1212/NXI.0000000000000962

3. Pascual-Goñi E, Caballero-Ávila M, Querol L. Antibodies in Autoimmune Neuropathies: What to Test, How to Test, Why to Test. *Neurology*. 2024;103(4):e209725. doi:10.1212/WNL.0000000000209725

4. Miske R, Scharf M, Borowski K, et al. Septin-3 autoimmunity in patients with paraneoplastic cerebellar ataxia. *J Neuroinflammation*. 2023;20(1):88. doi:10.1186/s12974-023-02718-9

5. Honorat JA, Lopez-Chiriboga AS, Kryzer TJ, et al. Autoimmune septin-5 cerebellar ataxia. *Neurol Neuroimmunol Neuroinflamm*. 2018;5(5):e474. doi:10.1212/NXI.0000000000000474

6. Hinson SR, Honorat JA, Grund EM, et al. Septin-5 and -7-IgGs: Neurologic, Serologic, and Pathophysiologic Characteristics. *Ann Neurol*. 2022;92(6):1090-1101. doi:10.1002/ana.26482

7. Herrero San Martin A, Amarante Cuadrado C, Gonzalez Arbizu M, et al. Autoimmune Septin-5 Disease Presenting as Spinocerebellar Ataxia and Nystagmus. *Neurology*. 2021;97(6):291-292. doi:10.1212/WNL.0000000000012240

8. Cavini IA, Leonardo DA, Rosa HVD, et al. The Structural Biology of Septins and Their Filaments: An Update. *Front Cell Dev Biol*. 2021;9:765085. doi:10.3389/fcell.2021.765085

9. Mostowy S, Cossart P. Septins: the fourth component of the cytoskeleton. *Nat Rev Mol Cell Biol*. 2012;13(3):183-194. doi:10.1038/nrm3284

10. Spiliotis ET, Nakos K. Cellular functions of actin- and microtubule-associated septins. *Curr Biol*. 2021;31(10):R651-R666. doi:10.1016/j.cub.2021.03.064

11. Ageta-Ishihara N, Kinoshita M. Developmental and postdevelopmental roles of septins in the brain. *Neurosci Res*. 2021;170:6-12. doi:10.1016/j.neures.2020.08.006

12. Patzig J, Erwig MS, Tenzer S, et al. Septin/anillin filaments scaffold central nervous system myelin to accelerate nerve conduction. *Elife*. 2016;5:e17119. doi:10.7554/eLife.17119

13. Erwig MS, Patzig J, Steyer AM, et al. Anillin facilitates septin assembly to prevent pathological outfoldings of central nervous system myelin. *Elife*. 2019;8:e43888. doi:10.7554/eLife.43888

14. Martens AK, Erwig M, Patzig J, Fledrich R, Füchtbauer EM, Werner HB. Targeted inactivation of the Septin2 and Septin9 genes in myelinating Schwann cells of mice. *Cytoskeleton (Hoboken)*. Published online November 15, 2022. doi:10.1002/cm.21736

15. Vorasoot N, Scharf M, Miske R, et al. CDR2 and CDR2L line blot performance in PCA-1/anti-Yo paraneoplastic autoimmunity. *Front Immunol*. 2023;14:1265797. doi:10.3389/fimmu.2023.1265797

16. Van den Bergh PYK, van Doorn PA, Hadden RDM, et al. European Academy of Neurology/Peripheral Nerve Society guideline on diagnosis and treatment of chronic inflammatory demyelinating polyradiculoneuropathy: Report of a joint Task Force-Second revision. *J Peripher Nerv Syst*. 2021;26(3):242-268. doi:10.1111/jns.12455

17. Menon MB, Sawada A, Chaturvedi A, et al. Genetic deletion of SEPT7 reveals a cell type-specific role of septins in microtubule destabilization for the completion of cytokinesis. *PLoS Genet*. 2014;10(8):e1004558. doi:10.1371/journal.pgen.1004558

18. Lappe-Siefke C, Goebbels S, Gravel M, et al. Disruption of Cnp1 uncouples oligodendroglial functions in axonal support and myelination. *Nat Genet*. 2003;33(3):366-374. doi:10.1038/ng1095

19. Arlt FA, Miske R, Machule ML, et al. KCNA2 IgG autoimmunity in neuropsychiatric diseases. *Brain Behav Immun*. 2024;117:399-411. doi:10.1016/j.bbi.2024.01.220

20. Arlt FA, Breuer A, Trampenau E, et al. High serum prevalence of autoreactive IgG antibodies against peripheral nerve structures in patients with neurological post-COVID-19 vaccination syndrome. *Front Immunol*. 2024;15:1404800. doi:10.3389/fimmu.2024.1404800

21. Appeltshauser L, Junghof H, Messinger J, et al. Anti-pan-neurofascin antibodies induce subclass-related complement activation and nodo-paranodal damage. *Brain*. Published online November 8, 2022:awac418. doi:10.1093/brain/awac418

22. Doppler K, Appeltshauser L, Villmann C, et al. Auto-antibodies to contactin-associated protein 1 (Caspr) in two patients with painful inflammatory neuropathy. *Brain*. 2016;139(Pt 10):2617-2630. doi:10.1093/brain/aww189

23. Dubowitz V, Sewry CA, Oldfors A. *Muscle Biopsy: A Practical Approach*. 5. Edition. Elsevier; 2021.

24. Preuße C, Allenbach Y, Hoffmann O, et al. Differential roles of hypoxia and innate immunity in juvenile and adult dermatomyositis. *Acta Neuropathol Commun*. 2016;4(1):45. doi:10.1186/s40478-016-0308-5

25. Dyck PJ, Thomas PK, eds. *Peripheral Neuropathy*. 4th ed. Saunders; 2005.

26. Abràmoff MD. Image Processing with ImageJ.

27. Schindelin J, Arganda-Carreras I, Frise E, et al. Fiji: an open-source platform for biological-image analysis. *Nat Methods*. 2012;9(7):676-682. doi:10.1038/nmeth.2019

28. Jaegle M, Ghazvini M, Mandemakers W, et al. The POU proteins Brn-2 and Oct-6 share important functions in Schwann cell development. *Genes Dev*. 2003;17(11):1380-1391. doi:10.1101/gad.258203

29. Manso C, Querol L, Mekaouche M, Illa I, Devaux JJ. Contactin-1 IgG4 antibodies cause paranode dismantling and conduction defects. *Brain*. 2016;139(Pt 6):1700-1712. doi:10.1093/brain/aww062

30. Hecker K, Grüner J, Hartmannsberger B, et al. Different binding and pathogenic effect of neurofascin and contactin-1 autoantibodies in autoimmune nodopathies. *Front Immunol*. 2023;14:1189734. doi:10.3389/fimmu.2023.1189734

31. Vural A, Doppler K, Meinl E. Autoantibodies Against the Node of Ranvier in Seropositive Chronic Inflammatory Demyelinating Polyneuropathy: Diagnostic, Pathogenic, and Therapeutic Relevance. *Front Immunol*. 2018;9:1029. doi:10.3389/fimmu.2018.01029

32. Querol L, Devaux J, Rojas-Garcia R, Illa I. Autoantibodies in chronic inflammatory neuropathies: diagnostic and therapeutic implications. *Nat Rev Neurol*. 2017;13(9):533-547. doi:10.1038/nrneurol.2017.84

33. Doppler K, Appeltshauser L, Wilhelmi K, et al. Destruction of paranodal architecture in inflammatory neuropathy with anti-contactin-1 autoantibodies. *J Neurol Neurosurg Psychiatry*. 2015;86(7):720-728. doi:10.1136/jnnp-2014-309916

34. Cortese A, Lombardi R, Briani C, et al. Antibodies to neurofascin, contactin-1, and contactin-associated protein 1 in CIDP: Clinical relevance of IgG isotype. *Neurol Neuroimmunol Neuroinflamm*. 2020;7(1):e639. doi:10.1212/NXI.0000000000000639

35. Querol L, Delmont E, Lleixà C. The autoimmune vulnerability of the node of Ranvier. *J Peripher Nerv Syst*. 2023;28 Suppl 3:S12-S22. doi:10.1111/jns.12570

36. Bergua C, Chiavelli H, Allenbach Y, et al. In vivo pathogenicity of IgG from patients with

anti-SRP or anti-HMGCR autoantibodies in immune-mediated necrotising myopathy. *Ann Rheum Dis*. 2019;78(1):131-139. doi:10.1136/annrheumdis-2018-213518

37. Pinal-Fernandez I, Muñoz-Braceras S, Casal-Dominguez M, et al. Pathological autoantibody internalisation in myositis. *Ann Rheum Dis*. 2024;83(11):1549-1560. doi:10.1136/ard-2024-225773

38. Siems SB, Jahn O, Eichel MA, et al. Proteome profile of peripheral myelin in healthy mice and in a neuropathy model. *Elife*. 2020;9. doi:10.7554/eLife.51406

39. Patzig J, Jahn O, Tenzer S, et al. Quantitative and integrative proteome analysis of peripheral nerve myelin identifies novel myelin proteins and candidate neuropathy loci. *J Neurosci*. 2011;31(45):16369-16386. doi:10.1523/JNEUROSCI.4016-11.2011

40. Hannibal MC, Ruzzo EK, Miller LR, et al. SEPT9 gene sequencing analysis reveals recurrent mutations in hereditary neuralgic amyotrophy. *Neurology*. 2009;72(20):1755-1759. doi:10.1212/WNL.0b013e3181a609e3

41. Kuhlenbäumer G, Hannibal MC, Nelis E, et al. Mutations in SEPT9 cause hereditary neuralgic amyotrophy. *Nat Genet*. 2005;37(10):1044-1046. doi:10.1038/ng1649

42. Ueda M, Kawamura N, Tateishi T, et al. Phenotypic spectrum of hereditary neuralgic amyotrophy caused by the SEPT9 R88W mutation. *J Neurol Neurosurg Psychiatry*. 2010;81(1):94-96. doi:10.1136/jnnp.2008.168260

43. Jahn O, Tenzer S, Bartsch N, Patzig J, Werner HB. Myelin Proteome Analysis: Methods and Implications for the Myelin Cytoskeleton. In: Dermietzel R, ed. *The Cytoskeleton: Imaging, Isolation, and Interaction*. Humana Press; 2013:335-353. doi:10.1007/978-1-62703-266-7_15

44. Clardy SL, Pittock SJ, Aktas O, et al. Network Meta-analysis of Ravulizumab and Alternative Interventions for the Treatment of Neuromyelitis Optica Spectrum Disorder. *Neurol Ther*. 2024;13(3):535-549. doi:10.1007/s40120-024-00597-7

45. Meisel A, Annane D, Vu T, et al. Long-term efficacy and safety of ravulizumab in adults with anti-acetylcholine receptor antibody-positive generalized myasthenia gravis: results from the phase 3 CHAMPION MG open-label extension. *J Neurol*. 2023;270(8):3862-3875. doi:10.1007/s00415-023-11699-x

46. Stengel H, Vural A, Brunder AM, et al. Anti-pan-neurofascin IgG3 as a marker of fulminant autoimmune neuropathy. *Neurol Neuroimmunol Neuroinflamm*. 2019;6(5):e603. doi:10.1212/NXI.0000000000000603

47. Doppler K, Schuster Y, Appeltshauser L, et al. Anti-CNTN1 IgG3 induces acute conduction block and motor deficits in a passive transfer rat model. *J Neuroinflammation*. 2019;16(1):73. doi:10.1186/s12974-019-1462-z

Figure legends

Figure 1 Autoreactive IgGs target septin multimers. (**A**) Representative images of indirect immunofluorescence on mouse sciatic nerve teased fibers showed reactivity of patient 1-3 serum to paranodes and paranodal myelin (arrowhead), as well as Schmidt-Lanterman incisures (asterisk). (**B**) Volcano plot representing significantly enriched proteins (labeled in black) in patient 1 IgG IP compared to a negative control; the x-axis displays the log2-transformed fold change, and the y-axis represents the -log10-transformed p-value. (**C**) IBAQs (intensity-based absolute quantification) of mass spectrometry-identified proteins in the IP of patient 1. (**D**) Cell-based assays with sera of patient 1,2, and 3 showed IgG reactivity against septin multimer overexpressing HEK293 cells, but not against untransfected control HEK293 cells. (**E-F**) Representative images of indirect immunofluorescence on unfixed rat brain sections showing IgG reactivity of serum 1 against the molecular layer of the hippocampus (**E**), and the molecular layer and white matter in the cerebellum (**F**). (**G**) Neutralization assays on brain tissue showed full absorbance of the IgG signal after preincubation with septin multimer HEK293 cell extracts, while preincubation with control HEK293 cells did not alter the tissue reactivity. Scale bar in A and D: 10 µm, Scale bar in E-G: 50 µm.

Figure 2 Septin multimer IgG demonstrate a characteristic binding pattern to PNS myelin. (**A-C**) Representative images of indirect immunofluorescence with serum of patient 1 and commercial SEPTIN2 and SEPTIN7 antibodies on sciatic nerve teased fibers demonstrated signal overlay at paranodal myelin of large caliber fibers (**A**), paranodes of small caliber fibers (**B**), and Schmidt-Lanterman incisures (**C**). (**D**) Indirect immunofluorescence of serum 1 on sciatic nerve teased fibers of *Septin7*-cKO mice lacking *Septin7* expression in Schwann cells. The serum demonstrated only weak axonal reactivity, while the commercial anti-SEPTIN7 antibody displayed axonal immunolabeling

(arrows) when SEPTIN7 was lacking from myelin. Three animals per genotype were stained per group and showed equal results as represented here. (**E**) Neutralization assays on WT nerves showing complete loss of serum binding upon preincubation with septin multimer HEK293 cell extracts. Sequential staining of non-absorbed commercial anti-SEPTIN2 and SEPTIN7 antibodies (magenta) indicate the presence of SEPTIN2 and -7 patterns. Scale bar in A-E: 10µm.

Figure 3 Septin multimer IgG bound to paranodes and Schmidt-Lanterman incisures of living myelinated axons. (**A** and **B**) Photomicrographs show serum binding of patient 1 (green), but not of a healthy control serum to nodo-paranodal structures in living cultured myelinating dorsal root ganglion cultures after five days of preincubation. The patient serum's binding partly colocalized with SEPTIN7 (A, magenta) and SEPTIN2 (B, magenta), which are expressed at the paranodes (arrowheads) and the Schmidt-Lanterman incisures (asterisk), as shown in the overlay image (merge). Note that staining with commercial SEPTIN antibodies was performed after fixation and permeabilization while serum preincubation was done on live cells. Overlay of both signals is in particular visible at the SEPTIN7 positive paranode. (**C**) Despite strong binding of the patient serum to the paranodes after five days of preincubation (yellow, left), the compact myelin, nodo-paranodal region (arrowheads), and Schmidt-Lanterman incisures showed no morphological alterations, as shown by anti-MAG staining (cyan) and anti-Neurofascin staining (magenta). Nodo-paranodal morphology was unaltered compared to staining after permeabilization without preincubation (yellow, middle) or after five days of preincubation of a healthy control serum (yellow, right). Scale bar in A-C: 10µm. All experiments were performed twice and no discrepancies in results were observed.

Figure 4 Complement binding and sural nerve inflammation. (**A**) Complement assay with septin multimer overexpressing HEK293 cells and control cells showed an overlay of patient 1 serum IgG staining and commercial human C3c antibody while a control serum without septin multimer IgGs showed no complement deposition, scale bar: 10µm. (**B**) C5b-9 immunohistochemical preparation illustrating MAC deposition on an endoneurial capillary (arrow); note the physiological complement deposition in the perineurium and on epineurial arterioles (original magnification x200). (**C**) H&E as well as Gömöri trichrome stains of a sural nerve fascicle highlighting edematous alterations and inflammatory infiltrates (CD68, CD45, CD8) predominantly in the perineurium (original magnification x200). Scale bars in B-C: 50µm.

Figure 5 Histopathological changes in myelin and axons in the sural nerve biopsy. [**A**(**i** and **ii**)] Semithin sections stained by methyleneblue illustrate acute axonal degeneration [e.g. black arrow in **A**(**ii**)] as well as hypomyelinated fibers [arrowheads in **A**(**i** and **ii**)]. In addition, small clusters of axonal regeneration are also detectable [black arrows in **A**(**ii**)] (original magnification x 600). [**B**(**i** and **ii**)] Fiber teasing shows myelin ovoids as signs of acute axonal degeneration [black arrows in **B**(**i**)], short segments – in comparison to the one above, indicative of re-myelination after primary demyelination [white arrowheads in **B**(**i**)]. Hypomyelinated shorter segments reflecting demyelination [black arrowheads in **B**(**ii**)]. Nodal/paranodal regions did not show any overt enlargement of the paranodal area; NR: Node of Ranvier (original magnification x100). (**C**) Ultrastructural analysis revealed loss of unmyelinated axons, illustrated by formation of collagen pockets (white arrows; original magnification x 12.000). (**D**–**F**) Representative images of indirect immunofluorescence on dermal punch biopsies of patient 1 showed both, reduced myelin staining (**D**, arrowheads), and elongated nodes/paranodes demonstrated by elongation of anti-pan-neurofascin immunoreactivity (**E**), as well as regular nodal and myelin architecture (**F**). Scale bar in A–D: 50µm, F-H: 10µm.

Figure 6 Immunotherapy and cell-based assay titers in serum of patient 1. (**A**) Grip strength measurement in kilogram (kg) of the left hand before initiation of the second plasma exchange cycle (April 7th 2022) until the day after the last plasma exchange treatment (April 28th 2022) within that cycle. Dots represent three replicates of grip strength assessments per day and lines show the mean of the daily measurements indicating a slight improvement upon treatment. (**B**) Modified ranking scale (mRS) of patients 1 (dots), 2 (rectangles), and 3 (polygon) at years after symptom onset. The arrow shows the initiation of intensified immunotherapy in patient 1 in May 2021. Patient 2 and 3 died without effective immunotherapy (†) after two years and 14 months, respectively. (**C**) Septin multimer autoantibody titers in serum of patient 1 from initiation of intensified immunotherapy onwards. Titers are displayed on a log10 scale. Black dots represent titers.

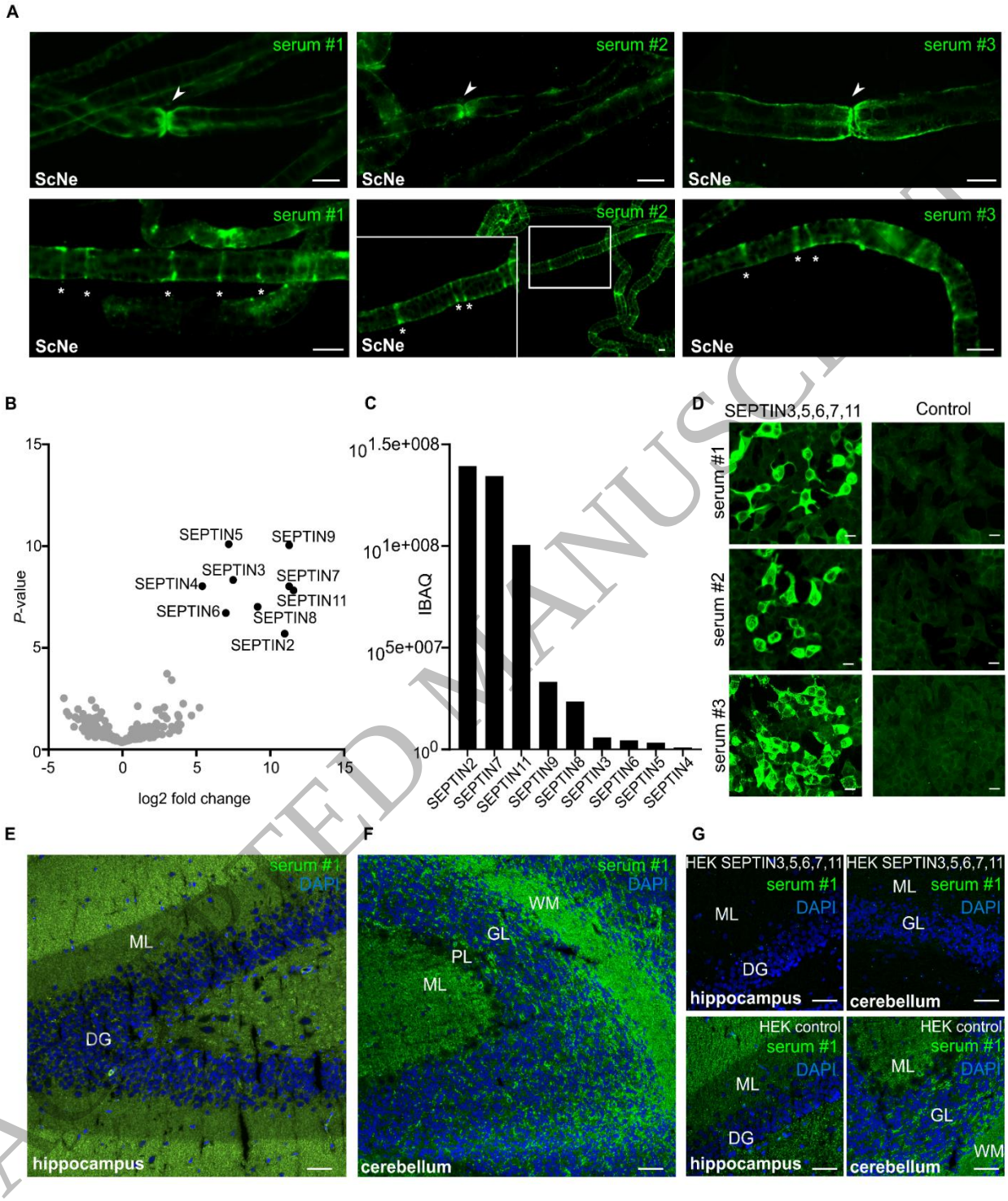

Figure 1
188x212 mm (x DPI)

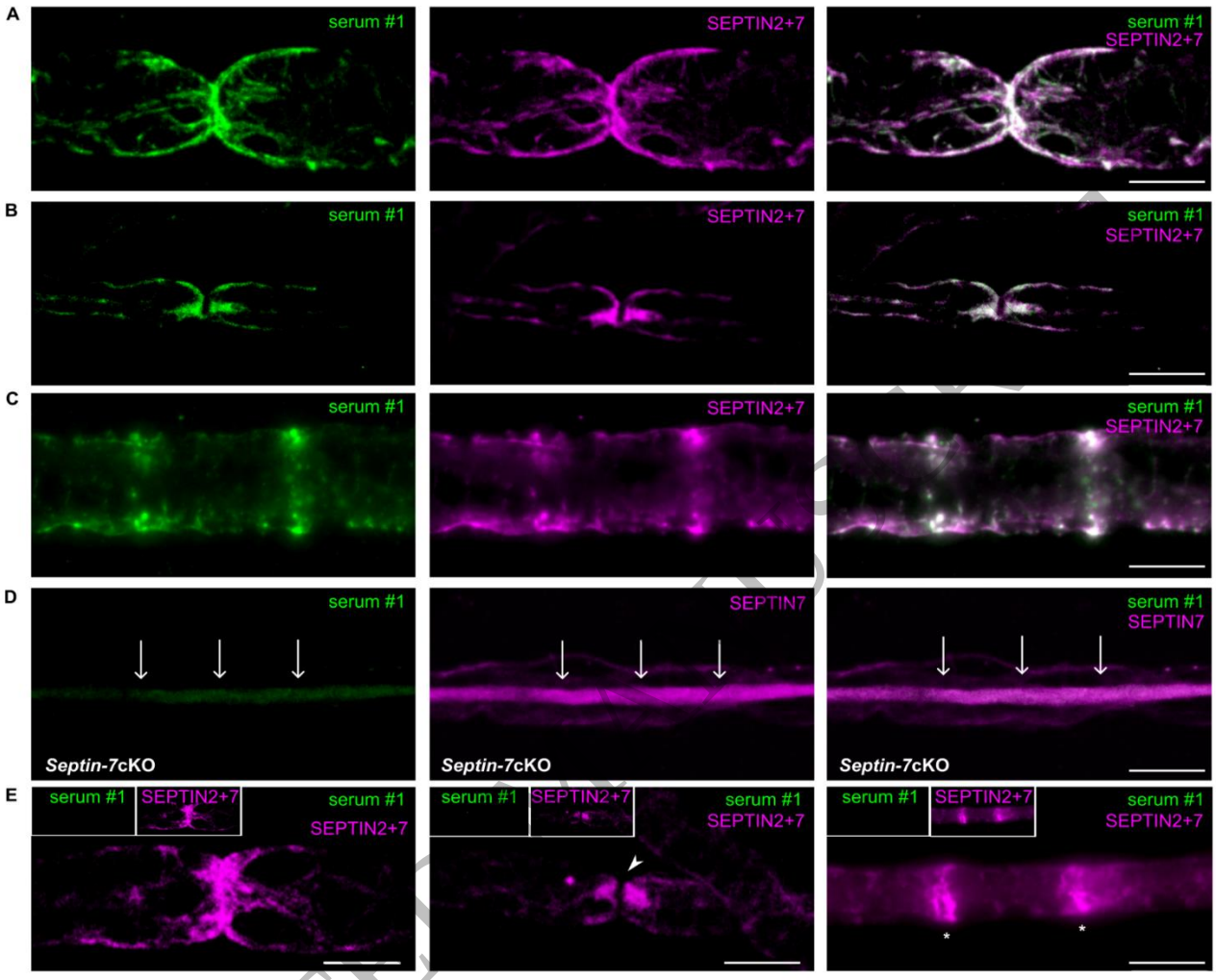

Figure 2
189x157 mm (x DPI)

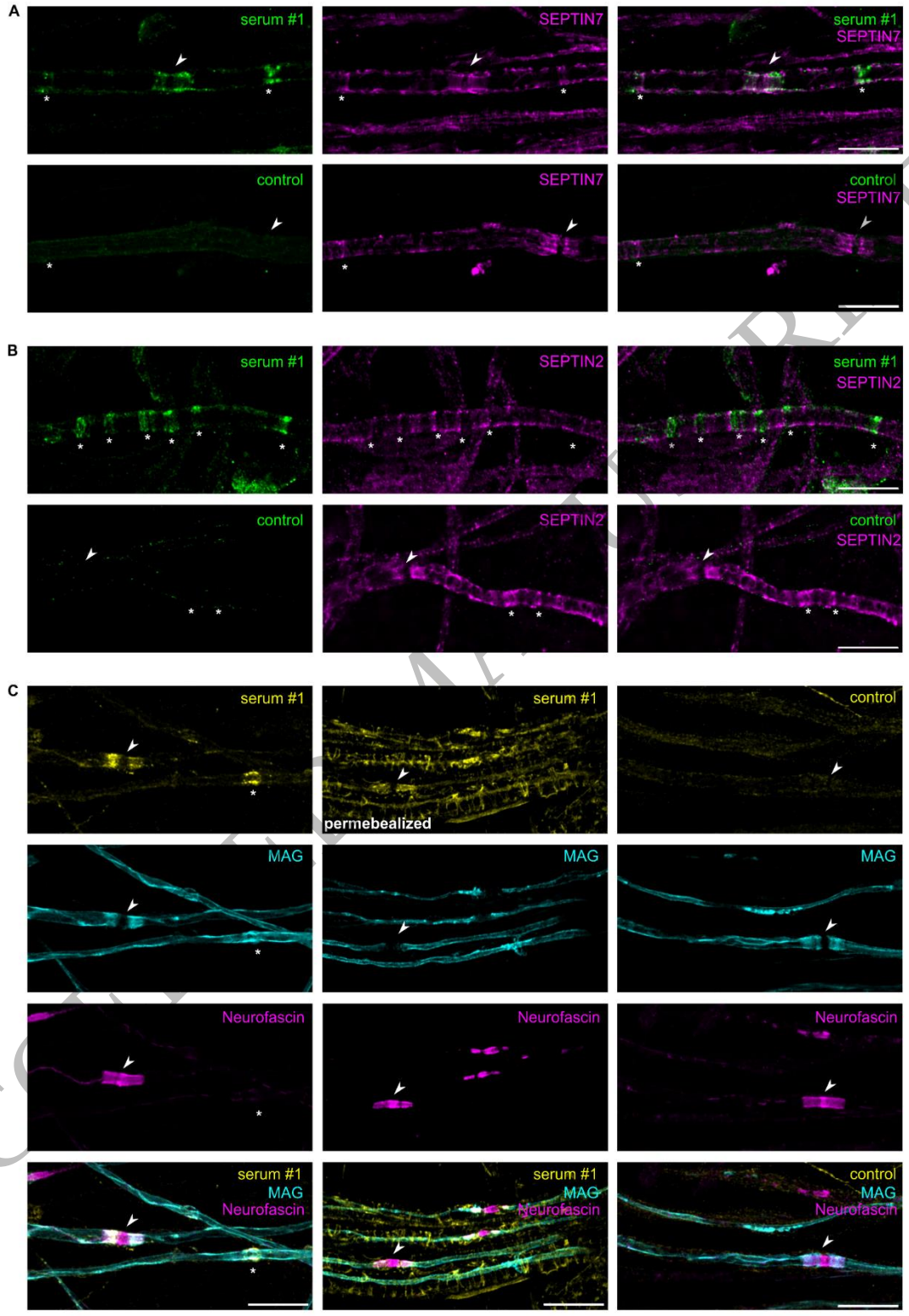

Figure 3
187x266 mm (x DPI)

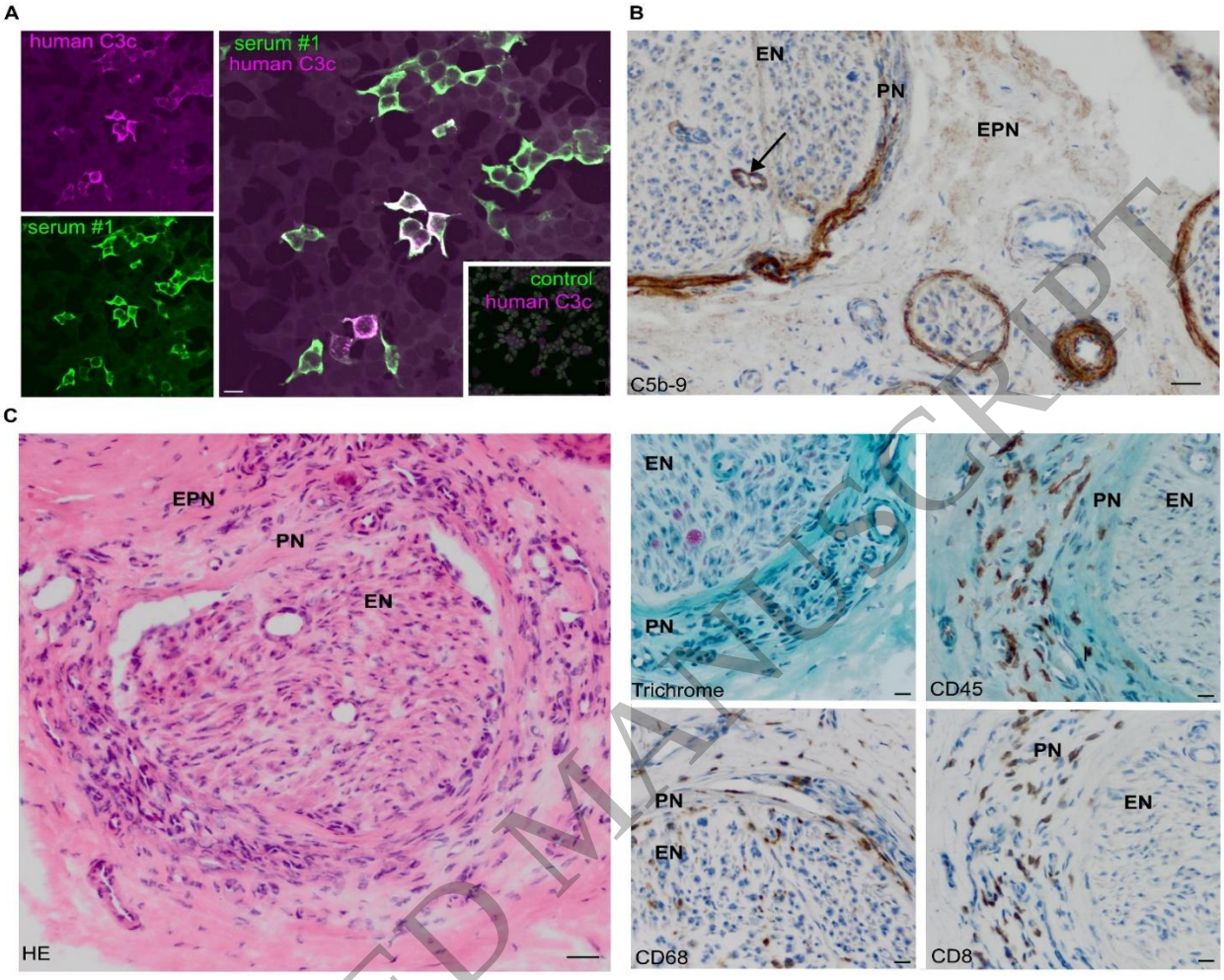

Figure 4
188x164 mm (x DPI)

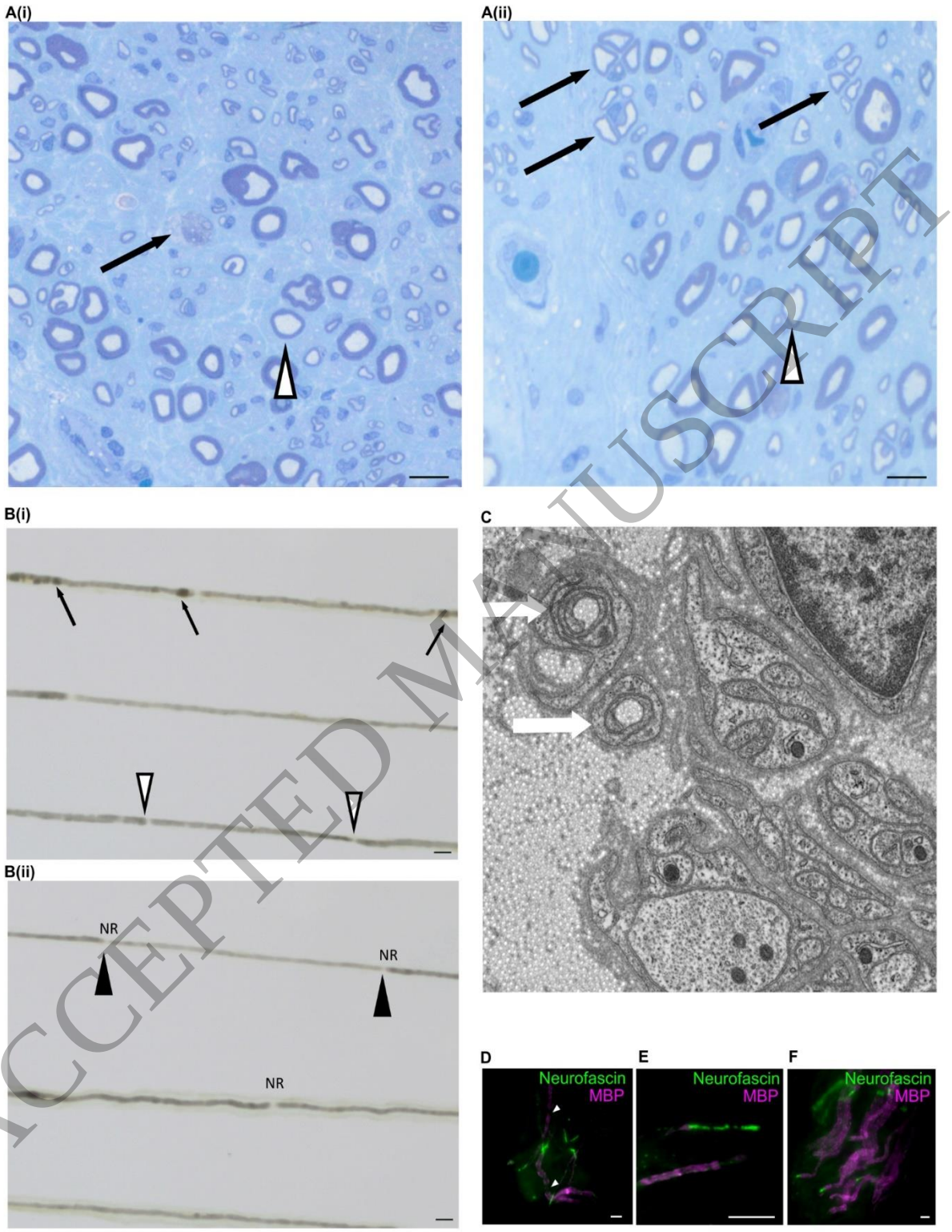

Figure 5
190x239 mm (x DPI)

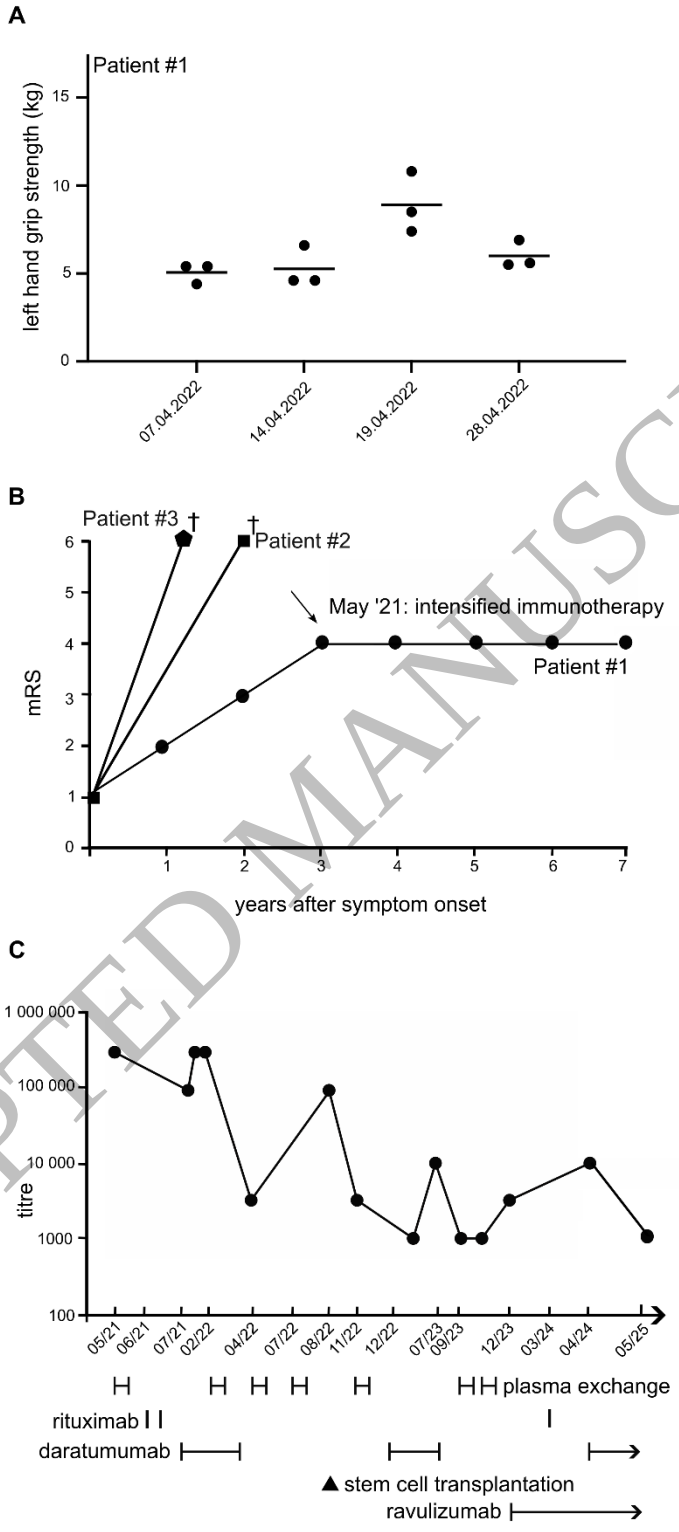

Figure 6
92x205 mm (x DPI)

1 **Table 1 Clinical data of patients with septin multimer autoantibodies**

Patient number, age, gender	Septin multimer CBA titre	Working Diagnosis	Clinical presentation	MRI	Electrophysiology	Nf-L serum Nf-L CSF CSF status Abs Serology	Immunotherapy, disease course, follow-up
#1, 65 years, male	1:320 000	Lower motor neuron disease	Progressive, asymmetric tetraparesis with fasciculations and atrophy (legs > arms), flail leg syndrome. Fine motor impairment of hands. Areflexia of lower limbs. Mild sensory symptoms with initial numbness, paraesthesia in legs (right>left, distal), progress to upper extremities.	Cerebral: normal Spine: no spinal cord atrophy	NCS: axonal > demyelinating, motor > sensory neuropathy. EAN/PNS electrodiagnostic criteria: possible CIDP. EMG: pathological spontaneous activity in upper and lower limb and paravertebrally. Motor evoked potentials: no sign of affection of 1st motor neuron.	23.3pg/ml (Ref.: <30.90pg/ml) 1140pg/ml (Ref.: <2500pg/ml) 1 cell/µl (0–4), protein CSF: 445.4mg/l (Ref.: 150–450)	Chronic onset, moderately progressive with subacute deteriorations (nadir within 4 years). Extensive immunotherapy (Fig. 6). Stabilization for 4 years.
#2, 72 years, male	1:100 000	Lower motor neuron disease	Progressive, asymmetric tetraparesis with limb cramps and atrophy (arms > legs), flail arm syndrome. Fine motor impairment of hands. Areflexia of upper extremities. No reported sensory symptoms.	Cerebral: normal Spine: no spinal cord atrophy	NCS axonal > demyelinating, motor-sensory neuropathy. EAN/PNS electrodiagnostic criteria: not fulfilled. EMG: pathological spontaneous activity in upper and lower limb and paravertebrally. Motor evoked potentials: no sign of affection of 1st motor neuron.	Nf-L serum/CSF n.d. 1 cell/µl (Ref.: 0–5), protein CSF: 37mg/dl (Ref.: 0–35) VGCC-P/Q: 0.05 nmol/l[a]	Chronic onset, moderately progressive (nadir within 2 years). No immunotherapy. Died 2 years after onset due to pneumonia with advanced stage motor impairment.
#3, 79 years, female	1:100 000	Lower motor neuron disease	Progressive, asymmetric tetraparesis (legs> arms), limb cramps, bilateral thenar muscle atrophy. Gait abnormalities with frequent falls. Dysphagia, vocal cord paralysis. Reflexes normal in both upper and lower limbs.	Cerebral: mild atrophy, moderate chronic small vessel ischemic changes, small old lacunar infarct in right thalamus and right caudate. Spine: multilevel spondylitis.	NCS: upper and lower axonal, motor > sensory neuropathy, left > right. EAN/PNS electrodiagnostic criteria: possible CIDP. EMG: normal. Motor evoked potentials: not performed.	Nf-L serum/CSF n.d. 2 cells/mm^3 (Ref: 0–5/mm^3), CSF protein 67mg/dl (ref: 15–45 mg/dl) VGCC-P/Q: 0.05 nmol/L[a]	Subacute onset, rapidly progressive, wheel-chair bound within 4 months. Died 14 months after onset due to infection (abdominal skin abscess/cellulitis) with PEG. Treated with IVIg 2g/kg over 5 days without reported benefit. Prednisolone taper dose without improvement.

			Mild, symmetric sensory symptoms in distal extremities (paraesthesia, dysesthesia).				One dose of rituximab without reported benefit.

Electrodiagnostic findings of NCS were initially interpreted as Carpal tunnel syndrome in Patients 1 and 2. Abs = autoantibodies; NCS = Nerve conduction studies; Nf-L = Neurofilament light-chain; n.d. = not done. PEG = percutaneous endoscopic gastrostomy Ref. = Reference value; VGCC-P/Q = voltage-gated calcium channel P/Q subunit.

[a]Staining with a high-positive VGCC-P/Q serum and commercial VGCC-P/Q antibody did not show a similar pattern to patient 1-3 serum on sciatic nerve teased fibres (Supplementary Fig. 7).